MXene Composite and Coaxial Fibers with High Stretchability and Conductivity for Wearable Strain Sensing Textiles

Shayan Seyedin,* Simge Uzun, Ariana Levitt, Babak Anasori, Genevieve Dion, Yury Gogotsi,* and Joselito M. Razal*

Dr. S. Seyedin, S. Uzun, A. Levitt, Prof. B. Anasori, Prof. Y. Gogotsi
A. J. Drexel Nanomaterials Institute,
Department of Materials Science and Engineering
Drexel University, Philadelphia, PA 19104, USA
Email: joselito.razal@deakin.edu.au, gogotsi@drexel.edu, s.seyedin@imperial.ac.uk

Dr. S. Seyedin, Prof. J.M. Razal
Institute for Frontier Materials
Deakin University
Geelong, VIC 3220, Australia

Dr. S. Seyedin
Molecular Sciences Research Hub
Imperial College London
London, W12 0BZ, UK

Prof. B. Anasori
Integrated Nanosystems Development Institute
Department of Mechanical and Energy Engineering
Purdue School of Engineering and Technology
Indiana University−Purdue University Indianapolis
Indianapolis, IN 46202, USA

Prof. G. Dion
Center for Functional Fabrics, Drexel University,
Philadelphia, PA 19104, USA

Abstract

The integration of nanomaterials with high conductivity into stretchable polymer fibers can achieve novel functionalities such as sensing physical deformations. With a metallic conductivity that exceeds other solution-processed nanomaterials, two-dimensional (2D) titanium carbide MXene is an attractive material to produce conducting and stretchable fibers. Here, we use a scalable wet-spinning technique to produce $Ti_3C_2T_x$ MXene/polyurethane (PU) composite fibers that show both conductivity and high stretchability. We demonstrate conductivity at a very low percolation threshold of ~1 wt.%, which is lower than the previously reported values for MXene-based polymer composites. When used as a strain sensor, the MXene/PU composite fibers show a high gauge factor of ~12900 (~238 at 50 % strain) and a large sensing strain of ~152 %. We further improve the cyclic strain sensing performance by producing fibers with MXene/PU sheath and pure PU core using a coaxial wet-spinning process. Using a commercial-scale knitting machine, we knit MXene/PU fibers into a one-piece elbow sleeve, which can track various movements of the wearer's elbow. This study establishes fundamental insights into the behavior of MXene in elastomeric composites and presents strategies to achieve MXene-based fibers and textiles with strain sensing properties suitable for applications in health, sports, and entertainment.

1. Introduction

MXenes are a large family of two-dimensional (2D) materials[1–5] with high electrical conductivity (up to ~10^4 S cm^{-1}),[6] outstanding mechanical properties (Young's modulus ~330 GPa),[7] and excellent specific capacitance (up to ~1500 F cm^{-3}).[8] Owing to this unique combination of properties, Ti_3C_2 MXene has found applications in energy storage, sensing, catalysis, antennas, and neural interfaces among many others.[4,5,9–12] Typically synthesized from the parent MAX phases ($M_{n+1}AX_n$ with "M" as early transition metals, "A" group 13-16 elements, "X" carbon and/or nitrogen, and n = 1–4) by etching the "A" layer, following an intercalation-assisted delamination,[13] MXene ($M_{n+1}X_nT_x$) flakes with high aspect ratio (up to ~10^6) and abundant terminating functional groups (T_x) are desirable for producing polymer composites with novel functionalities. For instance, $Ti_3C_2T_x$ MXene/sodium alginate composite films showed an electromagnetic interference shielding that exceeded other synthetic composite materials with similar thicknesses.[14] One important application where MXene can offer an advantage over commonly used fillers is in composite fibers that require electrical conductivity and elasticity at the same time. This combination of conductivity and stretchability is the fundamental requirement for sensing physical deformations such as strain. A variety of materials, including conducting polymers such as poly(3,4-ethylenedioxythiophene):poly(styrenesulfonate) (PEDOT:PSS),[15–18] carbon black (CB),[19] carbon nanotubes (CNT),[19] chemically converted graphene (CCG),[19] reduced graphene oxide (rGO),[19–21] and mixture of silver nanoparticles (AgNP) and nanowires (NW)[22,23] have been used as fillers to achieve strain sensing composite fibers. Once integrated into a fabric, such fibers can be used for tracking body movements, sports coaching, rehabilitation, remote health monitoring, and entertainment.[24]

The limited availability of strain sensing fibers that can be produced at a sufficiently large scale (>100 m) while meeting the mechanical properties requirements of industrial-scale textile

processes, such as knitting or weaving, has restricted their integration into strain sensing textiles for practical wearable applications. There are different methods to fabricate strain sensing textiles such as fiber spinning, coating on fibers, yarns, or fabrics and manipulating nanomaterials into stretchable yarns.[24] While coating is scalable and easy to achieve, the poor adhesion and mechanical properties mismatch between the fiber substrate and the coating layer often result in the degradation of the sensing response, especially for applications requiring large strains or numerous cycles.[24] Fiber-based strain sensors produced using the geometrical manipulation of functional materials (*e.g.,* CNT), such as wrapping, twisting, and coiling are typically fabricated at small (centimeter) scale, which will not be sufficient for integration into textile. Spinning conducting and elastomeric fibers prevents the delamination of conducting fillers by integrating them within elastomeric polymers, such as polyurethane (PU). This approach is also scalable and has shown potential in producing strain sensing fibers at a length beyond a kilometer.[18] However, imparting electrical properties while maintaining the stretchability in elastomeric polymer fibers has been a great challenge. This is because introducing conductive fillers often results in deterioration of spinnability (ability to form fibers) or can lead to fibers with low stretchability, which are not suitable for strain sensing applications.

While proven a promising candidate for the development of fibers and nanofibers with remarkable energy storage properties,[25–29] the suitability of MXene for developing strain sensing fibers remained unexplored. Previous works on film-based $Ti_3C_2T_x$ MXene composites have shown that it is possible to achieve conductivity albeit at high MXene loadings. For instance, $Ti_3C_2T_x$/polyvinyl alcohol (PVA) composite films showed a low conductivity of ~4 $\times$ 10^{-4} S cm^{-1} at the relatively high MXene loading of 40 wt.% while achieving low film stretchability (~4 %).[3] Similarly, $Ti_3C_2T_x$/cellulose nanofiber composite films showed a conductivity of only ~6 $\times$ 10^{-3} S cm^{-1} at 40 wt.% MXene.[30] While $Ti_3C_2T_x$/polyacrylamide

(PAM) composite films were conductive ($\sim3 \times 10^{-4}$ S cm^{-1}) at ~6 wt.% MXene, increasing the MXene loading to 75 wt.% only slightly improved the conductivity of the composite (~0.03 S cm^{-1}).[31] The recent study on Ti$_3$C$_2$T$_x$/PU did not report composite films with electrical conductivity.[32] Investigation of the mechanical properties of the Ti$_3$C$_2$T$_x$/PU composite films showed that a ~20 % increase in tensile strength at the low MXene loading of 0.5 wt.% was accompanied by a considerable decrease in strain at break from ~600 % in PU to ~500 % in the composite.[32] The previous studies on Ti$_3$C$_2$T$_x$ MXene composite films highlight the need for an in-depth understanding of MXene's behavior in composite systems to achieve fibers with balanced electrical and mechanical properties that are suitable for strain sensing application.

In this work, we show that Ti$_3$C$_2$T$_x$ MXene can be used to achieve highly conducting and stretchable fibers through a scalable wet-spinning process. We systematically study the effect of MXene loading on fiber spinnability and morphological, mechanical, and electrical properties of the MXene/PU composite fibers. We achieve a percolation threshold at ~1.0 wt.% MXene (volume fraction $\phi \approx 2.8 \times 10^{-3}$), which is significantly lower than the reported values for MXene-based composites (>6 wt.% MXene).[3,14,30,31] We show that the integration of MXene into PU results in a significant enhancement in Young's modulus (Y) of the fibers showing a high rate of reinforcement (dY/dϕ) of up to ~20.3 GPa. This dY/dϕ is higher than other PU-based composite fibers such as GO/PU[19–21] and CNT/PU[19] produced under similar conditions. When used as an individual fiber, the MXene/PU composite fiber can sense large strains (up to ~152%) with a high gauge factor (GF) of ~12900 (GF $\approx$ 238 at 50 % strain), which exceeds literature values for fiber-based strain sensors. We also produced coaxial fibers by using MXene/PU composite as the sheath and PU fiber as the core. This new fiber configuration further improved the sensing performance compared to conventional composite fibers especially when tested in cyclic stretching-releasing deformation. We show that the

outstanding mechanical properties of MXene/PU composite fibers enable their knitting into textiles using an industrial-scale knitting machine, similar to knitting of everyday yarns. The knitted textiles sense strains as large as 200 % with a GF of ~ -7.5, outperforming existing knitted textile strain sensors. Using the MXene/PU composite fibers, we knit an elbow sleeve that can readily monitor the diverse movements of a wearer by sending the signal to a personal computer. This work shows that the enhanced insight into the MXene's behavior in composite systems enables the fabrication of fibers that exhibit a unique combination of electrical conductivity and stretchability. It also shows that these MXene-based conducting elastomeric fibers can be integrated into strain sensing textiles for practical applications such as wearable body movement monitoring.

2. Results and discussion

We synthesized $Ti_3C_2T_x$ MXene using the minimally intensive layer delamination (MILD) method.[13] X-ray diffraction (XRD) results suggest complete etching of the Al layers of the Ti_3AlC_2 MAX phase and complete delamination of MXene layers (**Figure S1**). Investigation using the dynamic light scattering (DLS) technique revealed that ~78 % of the MXene flakes in the as-synthesized dispersion had an average size of ~0.58 µm, while there were ~6 % of larger flakes with an average size of ~5.21 µm; the average size of the remaining flakes was ~0.12 µm (**Figure S1c**). Since PU used in this work was insoluble in water, we used a solvent exchange method[33] to transfer $Ti_3C_2T_x$ MXene aqueous dispersion into dimethyl sulfoxide (DMSO) and dimethyl formamide (DMF) to achieve solvent compatibility with PU. In our initial investigation on drop-cast films, MXene/PU composite prepared in DMSO showed electrical conductivity at ~10 wt.% MXene, while the composite film cast from a DMF dispersion with the same loading of MXene was not electrically conductive. This could be due to a better intercalation of DMSO in $Ti_3C_2T_x$ MXene layers,[34] which leads to higher dispersibility. Hence, we used DMSO as the solvent and prepared spinning formulations at

various MXene loadings ranging from zero (pure PU) to 100 wt.% (pure MXene). **Table S1** in *Supporting Information* provides details of the formulations prepared for fiber spinning.

We used a wet-spinning technique, shown schematically in **Figure 1a**, to examine the spinnability of MXene/PU formulations into fibers. To elucidate the behavior of $Ti_3C_2T_x$ MXene in composite systems and its suitability to produce conducting elastomeric fibers, we systematically investigated the effect of MXene loading and spinning conditions on morphological, electrical, and mechanical properties of MXene/PU fibers. We used isopropanol (IPA) as the coagulating agent to prepare MXene/PU composite fibers.[16–21] **Figure 1b** shows a ~100-meter-long fiber at ~9.1 wt.% MXene loading collected continuously on a spool. We noticed that while IPA could be used as a coagulating agent to achieve fibers at MXene loading of up to ~28.6 wt.%, it resulted in poor coagulation at higher MXene loadings and thus frequent fiber breakages occurred. By substituting IPA with acetic acid (AcOH) in the coagulation bath, we achieved fibers throughout the whole range of MXene loading (0-100 wt.%). We used AcOH because it has previously shown to be a suitable coagulating agent for spinning MXene-based fibers.[25] Morphological investigation of the cross-section of the fibers using scanning electron microscopy (SEM) revealed that composite fibers spun in IPA coagulation bath at low loading of MXene (< ~9.1 wt.%) had irregular and ribbon-like cross-sections and surfaces, while AcOH resulted in fibers with relatively circular cross-sections (**Figure 1c**). Interestingly, more regular (circular) cross-section from the IPA bath was also achieved by increasing the MXene content in the fiber. This is because the shape of the cross-section of the fiber is predominantly governed by the rate of coagulation.[35] The fast rate of DMSO diffusion out of the spinning formulation into IPA resulted in a rapid coagulation to form irregular fiber surface morphology. In contrast, the outward diffusion of DMSO into AcOH was relatively slow (low rate of coagulation), producing circular fibers. These observations are in agreement with previous studies on other PU composites.[16,19,21] The

high dispersibility of $Ti_3C_2T_x$ MXene in polar solvents[36] facilitated the inward diffusion of IPA into the fiber with increasing MXene content, which led to more circular fibers.
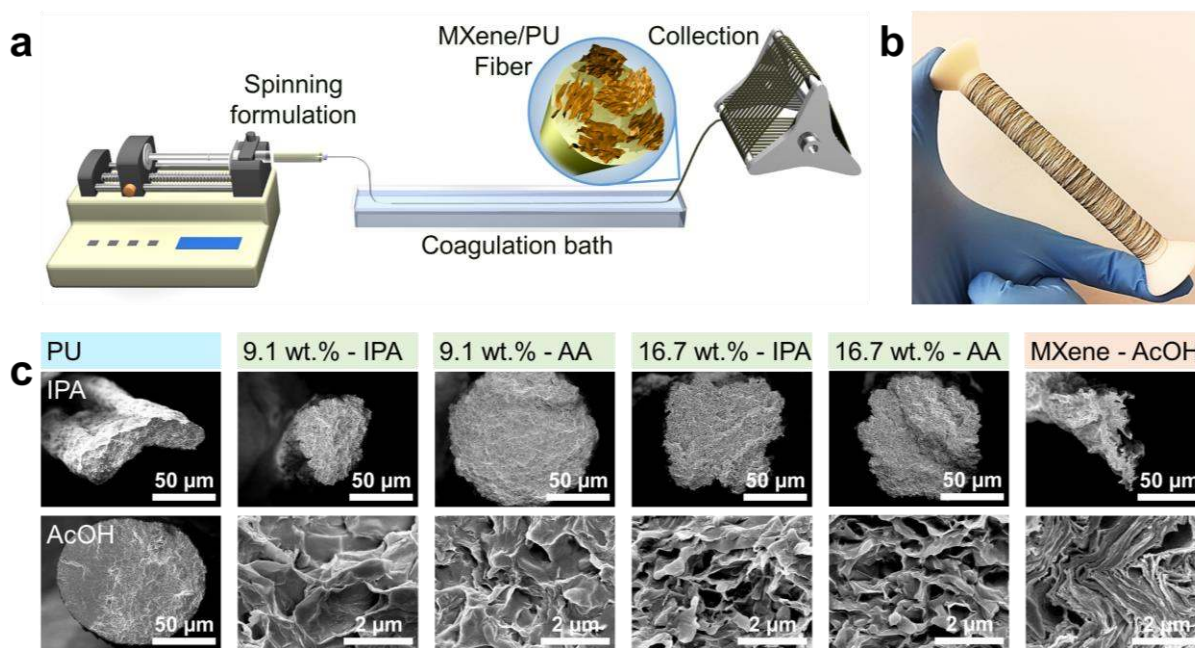

Figure 1. a) Schematic illustration of MXene/PU fiber spinning process, b) digital photograph of a ~100-meter-long MXene/PU fiber at ~9.1 wt.% MXene spun using IPA coagulation bath, and c) scanning electron microscopy (SEM) images of MXene/PU fibers produced at various MXene loadings and spinning conditions.

We measured the electrical conductivity of the composite fibers at various MXene loadings spun using IPA and AcOH coagulation baths (**Figure 2**). The onset of conductivity (percolation threshold) occurred at ~1.0 wt.% MXene loading for IPA spun fibers and at ~2.0 wt.% for fibers spun in AcOH. To our knowledge, this percolation threshold is the lowest value reported for MXene-based composites. The lowest reported percolation threshold was ~6 wt.% for MXene/PMMA composites.[31] The high intercalation of DMSO in $Ti_3C_2T_x$ MXene layers

compared to water and other organic solvents[34] and a planar geometry of MXene flakes in the

fiber could be the reason for the low percolation threshold observed in our composite fibers.

We also calculated volume fraction (ϕ) of $Ti_3C_2T_x$ MXene in the composite fibers by using

densities of 4.2 g cm^{-3} for MXene and 1.2 g cm^{-3} for PU[16,19–21] respectively. We observed that

the volumetric percolation threshold was $\sim 2.8 \times 10^{-3}$ for MXene/PU fibers spun in the IPA bath.

This is similar to the percolation threshold in the rGO/PU composite fiber system ($\sim 2.0 \times 10^{-3}$).[21] The use of MXene offers the advantage of eliminating the need for post-spinning

reduction treatment necessary to achieve conductive fibers when graphene oxide is used as the
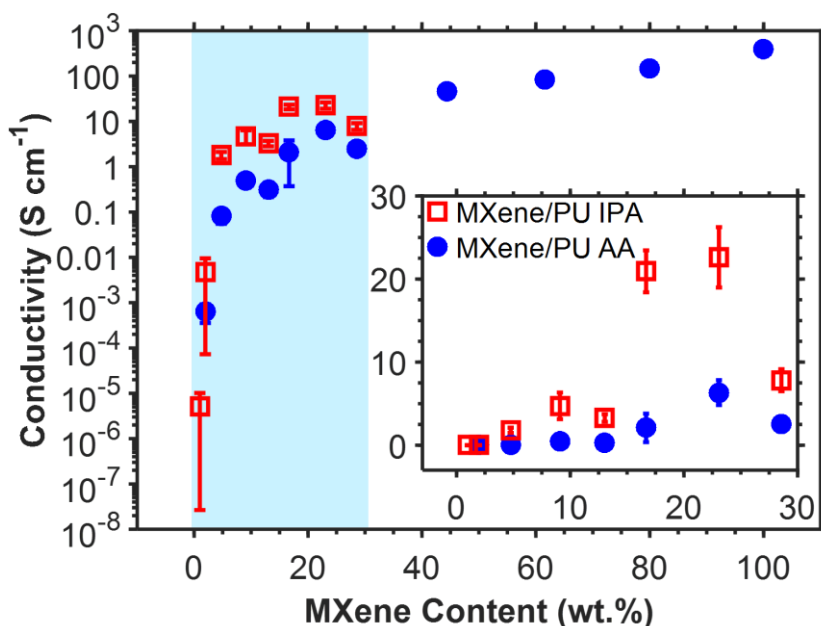
filler.

Figure 2. The effect of MXene loading on conductivity of MXene/PU fibers produced using

IPA and AcOH. The shaded area shows the region where fibers can be produced using the IPA

coagulation bath. The inset shows a linear increase in the MXene content of up to 30 wt.%.

The MXene/PU fibers spun from IPA showed higher conductivity than AcOH-spun fibers. This could be due to the faster coagulation rate of fibers in IPA (see discussions of mechanical properties), which resulted in less fiber stretching in the coagulation bath and thus minimized the separation of MXene flakes in the fiber. The conductivity of the fibers increased with MXene loading for both coagulation baths. For the IPA-spun fiber, the highest conductivity of ~22.6 S cm^{-1} was achieved at ~23.1 wt.% MXene loading. The AcOH-spun fiber at similar loading showed a lower conductivity of ~6.3 S cm^{-1}, which continued to increase with MXene loading until a conductivity of ~392 S cm^{-1} was achieved for the pure MXene fiber (100 wt.% MXene). This fiber conductivity is slightly less than the conductivity of ~515 S cm^{-1} measured for the free-standing MXene film obtained by vacuum filtration of the same MXene dispersion. Since the fiber spinning conditions used in this work were not optimized for pure MXene, the resulting fiber was porous (**Figure 1c**) and had lower conductivity than that of the film. We also compared the conductivity of fibers produced in this work with other PU composite fibers[16,19–21] fabricated under similar spinning conditions (**Figure S4**) and found that at the same filler loading, the conductivity of MXene/PU fiber is higher than that of CB/PU,[19] SWCNT/PU,[19] CCG/PU,[19] and rGO/PU fiber,[19–21] and is similar to PEDOT:PSS/PU fiber.[15–18]

We evaluated the mechanical properties of the MXene/PU fibers spun under various conditions by using uniaxial tensile testing. The stress-strain curves showed three distinct behaviors (**Figure 3a)** when the MXene loading was less than ~9.1 wt.% (**Figure 3b**), *i.e.*, an initial stiff response (region I), strain-induced softening (region II), and strain-induced hardening (region III). These regions are typical for filled elastomers.[16,19–21,37–40] The PU chains consist of two components: soft segments (SS) that form an amorphous phase providing large elongation and hard segments (HS) that cluster into ordered hard domains imparting stiffness.[37–41] This two-phase microstructure is responsible for the presence of the three regions illustrated in **Figure**

WILEY-VCH

3a. Here, the rigid HS domains result in a stiff response in region I. The extension of SS chains initially causes strain-induced softening (region II) while further stretching of PU increases the alignment of SS chains and ultimately leads to SIC of SS phase (region III).

The fibers with MXene loading above ~9.1 wt.% only showed the stiff region. The stress-strain curves of the fibers in the stiff region revealed a significant reinforcement (increase in stiffness) effect from MXene (**Figure 3c**). The Young's modulus (Y) of the IPA-spun fibers increased from ~7.1 MPa for pure PU to ~1145 MPa for MXene/PU at ~28.6 wt.% loading (ϕ=0.085). This is equivalent to a rate of reinforcement (dY/dϕ) of ~20.3 GPa. Similarly, for AcOH-spun fibers, a steady increase in Y from ~16.2 to ~5997 MPa was observed when MXene loading increased from zero to ~80.0 wt.% (dY/dϕ ~15.8 GPa). The increase in Y in MXene/PU fibers with increasing MXene content can be due to the so-called hydrodynamic effect[42–45] created as the result of the addition of MXene fillers with significantly higher stiffness than the soft PU host. The rate of reinforcement achieved for the MXene/PU fibers (~20.3 GPa) are higher than dY/dϕ for other composite fibers produced under similar conditions (**Figure S4**) such as GO/PU[20,21] (~15.8 GPa), CCG/PU[19] (2.1 GPa), and SWCNT/PU[19] (6.5 GPa). We noted that pure MXene fibers showed a significantly lower Young's modulus (~2750 MPa) than the composite fiber with ~80.0 wt.% MXene. This indicates that the interaction between PU and MXene flakes are stronger than the bonding between pure MXene flakes.
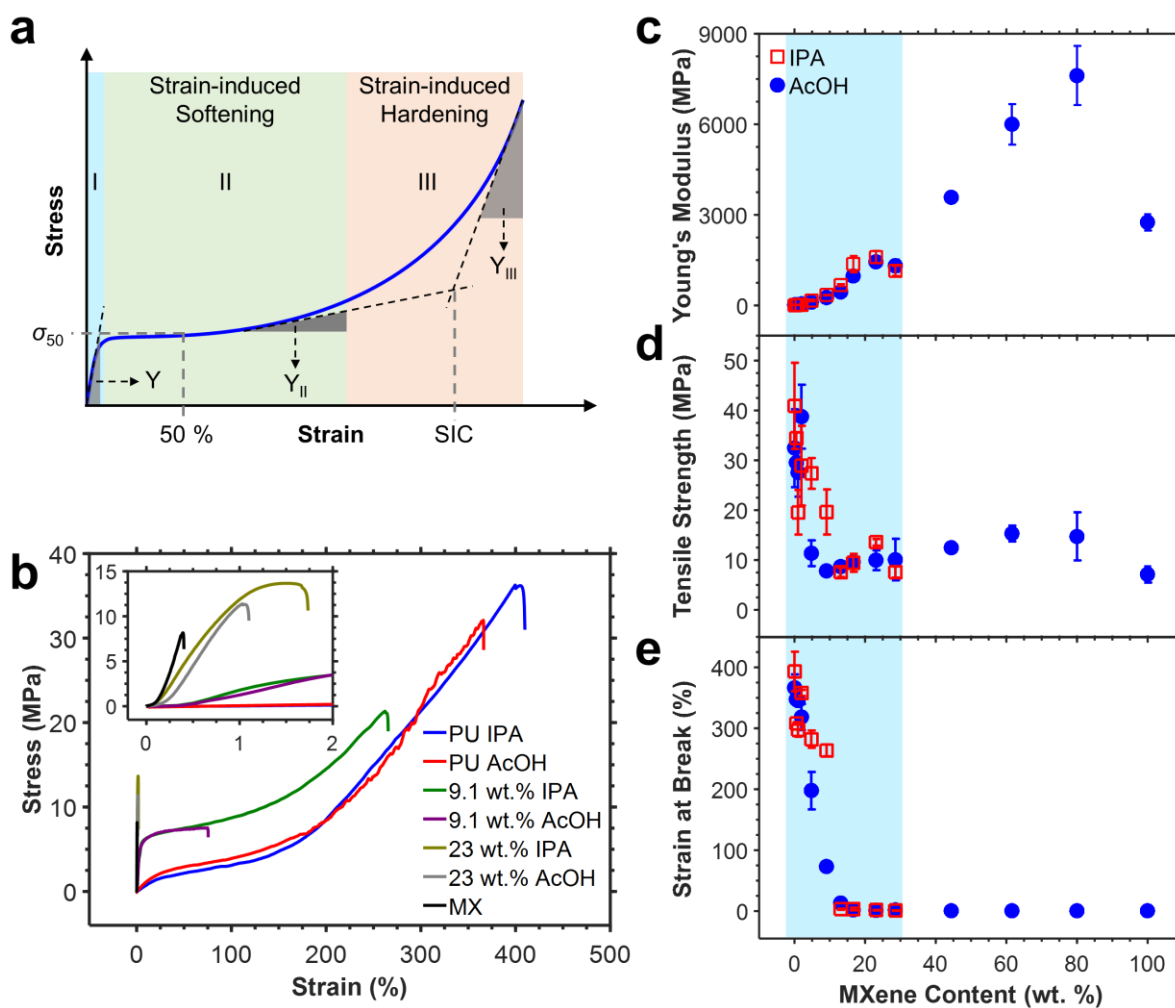
Figure 3. a) Schematic illustration of various stages of stress-strain curves for MXene/PU fibers, b) stress-strain curves of representative fibers, c) Young's modulus, d) tensile strength, and e) strain at break of MXene/PU fibers produced at various MXene loadings and spinning conditions. The shaded area in (c-e) shows the region where fibers can be produced using the IPA coagulation bath.

To quantify the strain-induced softening behavior of the fibers (region II), we calculated stress at 50 % strain (σ_{50}) and modulus in the strain range of 50-100 % (Y_{II}). The σ_{50} of MXene/PU fibers increased approximately three times when MXene loading increased from zero to ~9.1

wt.%, while Y_{II} remained relatively unchanged (**Figure S5**). The ability to incorporate fillers in PU without significantly disrupting SS extensibility or SIC is important for achieving reinforcement while utilizing the stretchability of PU. In our MXene/PU fibers with MXene loading of up to ~9.1 wt.%, the increase in σ_{50} indicates that introducing MXene into PU results not only in stiffness reinforcement, but also in strengthening of the fiber in the medium strain region (50-100 %). This strengthening will be beneficial for great majority of practical applications where fibers are subjected to limited stretching (<100 %).

In region III (strain above 200 %), stretching of the fibers resulted in a significant rise in stress (**Figure 3b**) due to the strain-induced crystallization (SIC). Interestingly in this region, there was no significant change in the modulus (Y_{III}) of the MXene/PU fibers with increasing the MXene loading from zero to ~9.1 wt.% (**Figure S5**). To quantify the SIC behavior of the MXene/PU fibers, we measured the strain at the intersection of the tangent lines of the stress-strain curves in regions II and III (**Figure 3a**). This SIC strain only showed a slight decrease with MXene loading (up to ~9.1 wt.%) in MXene/PU fibers (**Figure S5**). For instance, the SIC strain of ~182 % for PU decreased to ~160 % for MXene/PU (~9.1 wt.%). A combination of relatively unchanged Y_{II} and Y_{III} and slight decrease in SIC strain indicate that the addition of MXene has minimal effect on the SS extensibility and does not disrupt the SIC of the SS in the PU host.

We observed that the strain at break (ε_B) and the tensile strength (σ_T) of the fibers decreased with MXene loading (**Figure 3d-e**). For IPA-spun fibers, ε_B decreased from ~393 % to ~264 % and σ_T decreased from ~40.9 to ~19.6 MPa with increasing MXene content from zero to ~9.1 wt.%. The AcOH-spun fibers showed lower ε_B and σ_T than the IPA-spun fibers. For instance, the AcOH-spun fiber at ~9.1 wt.% MXene showed ε_B and σ_T of ~73.1 % and ~7.8 MPa, possibly because the slow coagulation in AcOH could result in more stretching of SS

chains and longer MXene flakes sliding within the fiber during the spinning process. Further increase in MXene loading above ~9.1 wt.% resulted in brittle fibers that showed low stretchability and moderate strength (ε_B < 15 % and σ_T <10 MPa). The decrease in ε_B and σ_T of MXene/PU fibers at MXene loading more than ~9.1 wt.% is likely due to the enhanced interactions between MXene flakes, similar to the aggregation effect[46] observed in CNT polymer composite systems and interruption of SS extension. Assessment of composite fiber cross-section at breakage after stretching using SEM did not show obvious pullouts (**Figure S6**) indicting strong interfacial interaction of MXene and PU.

The above results indicate that by carefully choosing MXene content and spinning conditions, it is possible to produce MXene/PU composite fibers that represent the prominent attributes of their parent materials, *i.e.*, high stretchability inherent to PU and high electrical conductivity inherent to MXene. This unique combination of properties is desirable for strain sensing and many other applications. We evaluated the strain sensing performance of the MXene/PU composite fibers produced under various conditions by real-time monitoring of the change in resistance (R) during uniaxial tensile stretching. Investigation of the electromechanical properties of the fibers, shown in **Figure 4a** for representative samples, revealed an increase in $\Delta R/R_0$ with stretching (R_0: initial resistance) indicative of strain sensing behavior. We measured the sensing range and the gauge factor (GF) of the MXene/PU fibers (**Figure 4c-d**). The sensing range indicates the minimum and maximum strains, where the sensor performs and GF, calculated using equation 1, is a measure of the sensitivity of the sensor. We note that both the sensing range and GF, increased initially with MXene loading and then decreased with their peak values occurring at ~9.1 wt.% MXene for fibers spun in IPA (~4.8 wt.% for AcOH-spun). The IPA-spun ~9.1 wt.% MXene/PU fiber showed a sensing range of ~152 % strain and a high GF of ~12900 (GF ≈ 238 at 50 % strain), which are due to the combination of high stretchability (**Figure 3a**) and reasonably high electrical conductivity (**Figure 2**). This GF shows the high

sensitivity of the ~9.1 wt.% MXene/PU fiber sensor and exceeds the highest published values for fiber-based strain sensors such as PEDOT:PSS/PU monofilament[16] (GF $\approx 10^4$) and multifilament[18] (GF $\approx$ 1500), graphene nanoplatelets/PVA coated rubber yarn[47] (GF $\approx$ 1800) and AgNW-AgNP/poly(styrene-*b*-butadiene-*b*-styrene) (SBS) fiber[22] (GF $\approx$ 15).
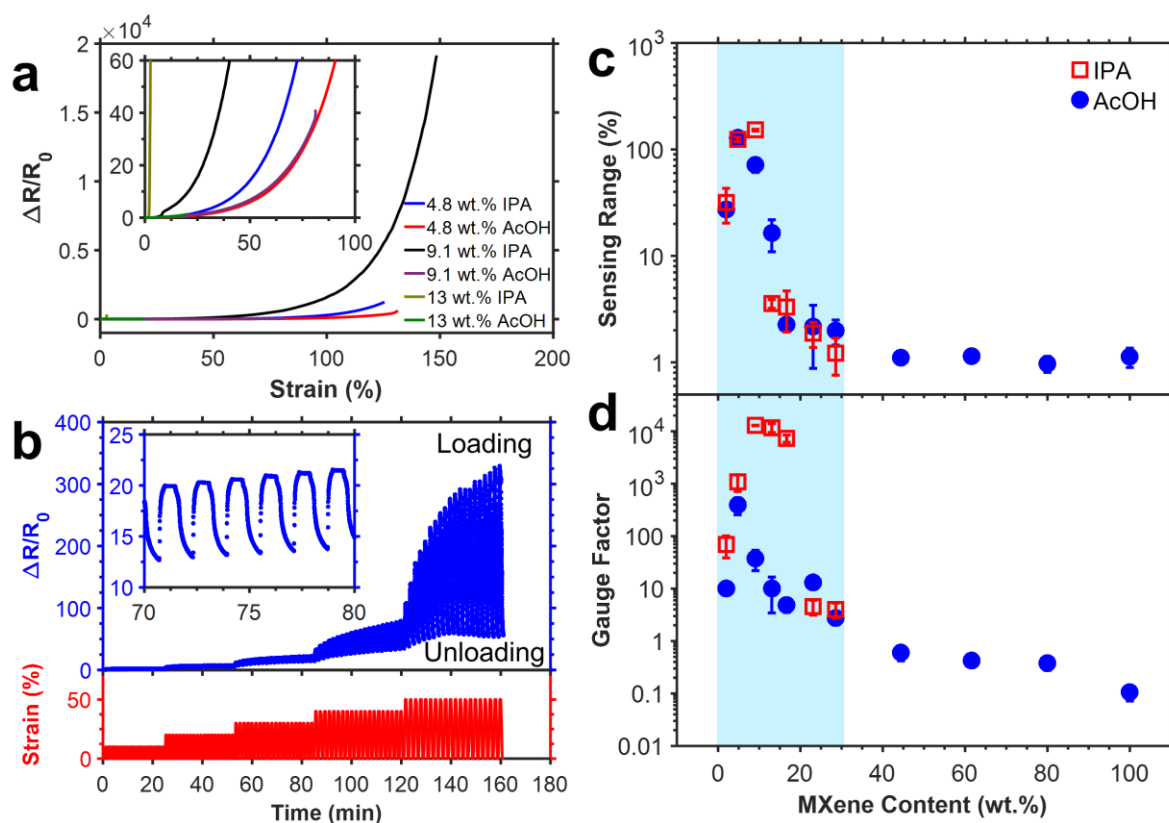

Figure 4. a) Strain sensing behavior of various MXene/PU fibers under uniaxial tensile stretching. b) Electromechanical properties of a representative MXene/PU fiber at ~9.1 wt.% MXene produced using IPA coagulation bath under cyclic stretching-releasing deformation at various strain magnitudes. Inset in (b) shows cyclic electromechanical properties of the same fiber at 30% strain for six cycles. c) Sensing range and d) gauge factor values for various MXene/PU fibers calculated from (a). The shaded area in (c-d) shows the region where fibers can be produced using the IPA coagulation bath.

We further investigated the strain sensing behavior of the IPA-spun fiber during repeated stretching-relaxing deformations (**Figure 4b**). In cyclic deformations, this fiber showed an increase in resistance during stretching (loading) and a decrease in resistance when relaxed to zero strain (unloading). Notably, the fiber sensor could detect incremental increases in applied strain by showing a larger difference between loading and unloading resistances. Stretch-induced changes in the conduction network[24] are considered to be the main reason for strain sensing behavior of the composite fibers. In this composite system, the disruption of interconnected MXene flakes results in increased resistance. This conduction network is restored when strain is removed, leading to decrease in resistance to the initial value. The high conductivity of MXene flakes enabled the formation of conduction network at a very high stretching of ~152 %, leading to high sensing range in the MXene/PU composite fiber. The high GF of the composite fiber can be explained by high stretching-induced changes in conduction network as a result of strong interaction between MXene flakes and PU chains, which gave rise to significant changes in resistance with stretching. The loading at which balanced stretchability and conductivity are achieved depends on the onset of SS extensibility interruption in PU as the result of filler particle addition, which were observed at loadings of ~13 wt.% and ~2.9 wt.% for PEDOT:PSS[16] and GO,[21] respectively. The realization of high stretchability and conductivity at the MXene loading of ~9.1 wt.% agrees well with previous works, given the smaller flake size of MXene compared to GO (average lateral size ~12 µm). The sensor responded well to cyclic strains of up to ~50 %, which was lower than the strain range of ~152 % measured in uniaxial tensile stretching deformation. We also observed a drift in the resistance response, which became more prominent with increasing the strain magnitude. The drift in the resistance response can be explained by the unrecoverable loss of conducting network due to the slippage or breakage of some of the MXene flakes during stretching, which results in only partial recovery of the conducting network during unloading.

16

We next used a coaxial wet-spinning approach (**Figure 5a**) and produced sheath/core fibers that consisted of a pure PU fiber as the inner core with the outer sheath of MXene. We used AcOH as the coagulation bath to produce coaxial fibers because the earlier results showed that IPA failed to generate MXene-based fibers with high MXene loading. While it was possible to produce a coaxial fiber with pure MXene layer as the sheath, we noticed that even small amount of stretching (~5%) resulted in permanent formation of cracks in the MXene layer and loss of conductivity. By making the outer layer a MXene/PU composite instead of pure MXene (**Figure 5b**), we achieved a coaxial fiber that showed a maximum sensing range of ~175 % strain with a GF of ~2300 during uniaxial tensile stretching (**Figure S7**). Analysis of the cross-section morphology of the coaxial fiber using SEM showed that there was a good adhesion between the outer MXene/PU composite layer with the inner PU core (**Figure 5c-d**). Additionally, by making coaxial fibers, we were able to use a higher MXene content of ~16.7 wt.% in the sheath to take advantage of its higher conductivity, while still possessing the elasticity of the PU core.

We also evaluated the cyclic strain sensing behavior of the coaxial fiber during repeated cyclic stretching-releasing test and observed that this fiber could sense various applied strain magnitudes of up to 150 % (**Figure 5e-f**). This is significantly higher than the 50 % strain sensing range achieved during cyclic stretching of non-coaxial composite fiber. The coaxial fiber also showed a smaller drift than the non-coaxial composite fiber and an improved stability in the cyclic sensing response at each applied strain magnitude. The enhancements in the cyclic sensing performance could be attributed to the high strain recovery of the core PU fiber, which helped the outer composite sensing layer restore the conduction network during unloading. This is evident from the cyclic extension-relaxation curves (**Figure S8**), which show residual strains of ~19 % and ~15 % at the applied strain of 50 % for the MXene/PU composite fiber (~9.1 wt.%) and the MXene/PU coaxial fiber, respectively. With higher sensing range,

sensitivity, and stability under repeated stretching-releasing deformations, the coaxial fiber offers a more practical sensing platform as an individual fiber, *i.e.*, not woven or knitted, than the composite fiber.
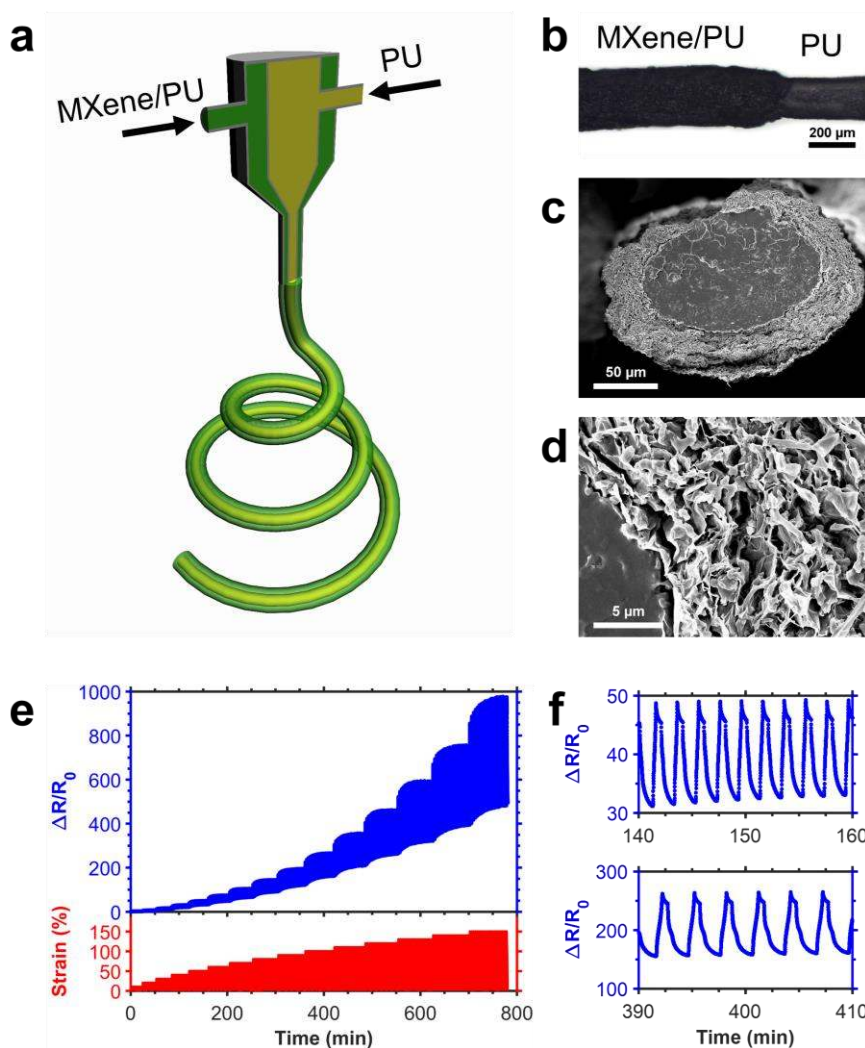

Figure 5. a) Schematic illustration of the coaxial fiber spinning approach used to achieve fibers with MXene/PU sheath and PU core. b) Optical microscopy image and c-d) SEM images of a MXene/PU coaxial fiber produced using MXene loading of ~16.7 wt.% in the sheath. The dark gray solid area on the left in (d) shows the MXene/PU composite outer sheath and the thinner fiber in the right side shows the inner PU core. e) Electromechanical properties of the MXene/PU coaxial fiber under cyclic stretching-releasing deformation at various applied strains. f) 20 min sections of $\Delta R/R_0$ in (e) for 50 % and 100 % strains.

The ability of the fiber to be knitted using an industrial-scale knitting machine is necessary to manufacture textile strain sensors that can be comfortably worn similar to everyday clothing. We examined the feasibility of integrating the composite fibers into a textile strain sensor device by knitting them on an industrial weft knitting machine. We used a single jersey knit structure (plain knit) and prepared two textile prototypes (~4 cm × ~1 cm) by knitting single and four-ply yarn of the composite fiber. We found that the composite fiber could withstand the high mechanical forces applied during industrial-scale knitting and could bend around successive knitting needles to form a series of intermeshing loops needed to produce fabrics (**Figure 6a-b**). We noticed that the textile produced by knitting four-ply yarn showed more uniform and packed loops than the knit made of single fiber likely due to the relatively small diameter of the single fiber (~115 µm) and the low needle gauge used for knitting (15 G).
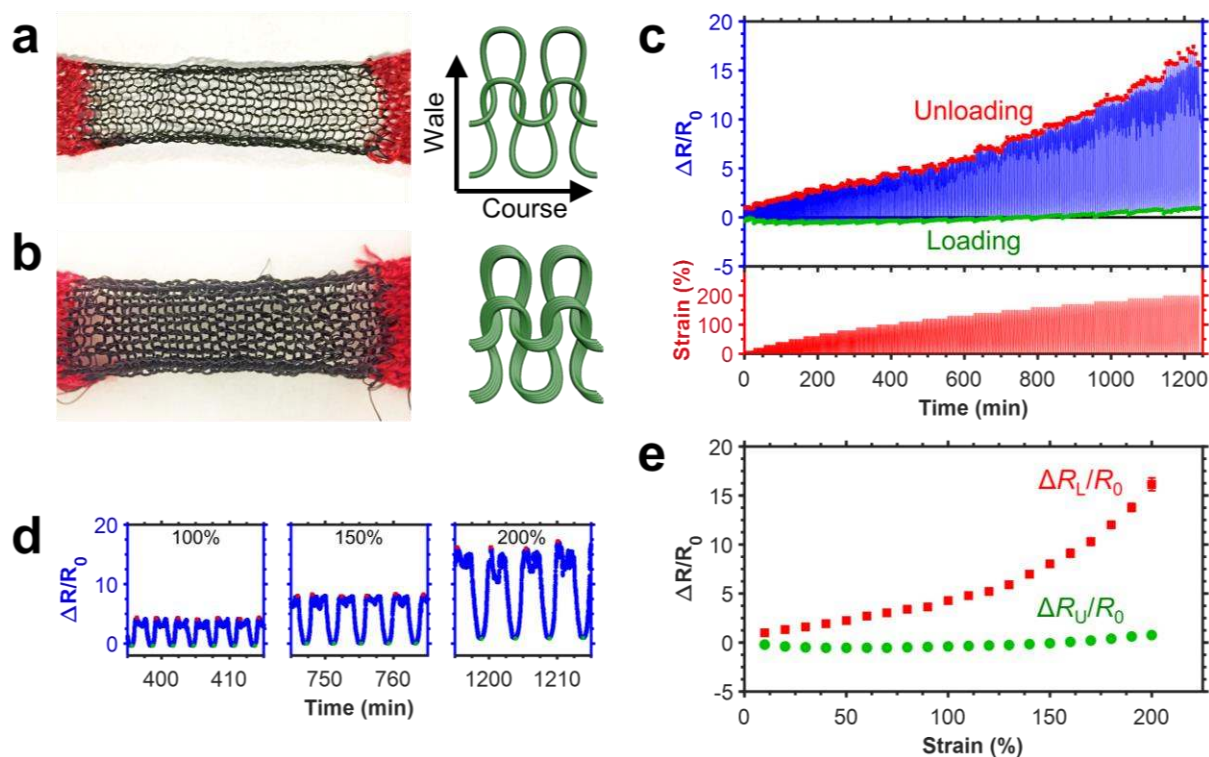
Figure 6. Single jersey textiles knitted by using a) single and b) four-ply yarn of MXene/PU composite fiber with ~9.1 wt.% MXene loading and their schematic illustrations. c) Electromechanical properties of the textile knitted using MXene/PU four-ply yarn under cyclic stretching-releasing deformation at various applied strains. d) 20-min sections of $\Delta R/R_0$ in (c) for 100 %, 150 %, and 200 % strains. e) $\Delta R/R_0$ for loading (R_L) and unloading (R_U) at each cycle.

We studied the strain sensing behavior of the textile knitted from four-ply yarn (four individual fibers) by monitoring its resistance change during cyclic stretching-releasing deformations in the wale direction (**Figure 6c**). We observed that the resistance of the textile decreased upon loading and increased when relaxed, resulting in a negative GF (**Figure 6c-d**), in contrast to the sensing behavior of the individual fibers that showed the opposite trend with positive GFs (**Figure 4b**). This is in agreement with our previous study[24] and can be explained by the

decrease in contact resistance between the interlocked fibers in textiles with stretching, which results in a decrease in the resistance response of the textile sensor. The knitted textile could sense strains of up to 200 % strain, which well exceeds the strain range required for wearable sensing reported as 55 % strain.[48] We also measured $\Delta R/R_0$ for loading ($\Delta R_L/R_0$) and unloading ($\Delta R_U/R_0$) at each cycle and observed that their difference increased with applied strain, indicating the sensor's ability to distinguish various levels of stretching. At 200 % strain, this difference can be translated to a GF of ~ -7.5 which is significantly higher in value compared to previous knitted textile strain sensors, which achieved GFs of up to -1.[17,18,49,50] In addition, the knitted textile sensor made with the ~9.1 wt.% MXene/PU four-ply yarn showed a high stability by maintaining its sensing response during loading and unloading for 1000 cycles of stretching-releasing deformations at 50 % strain (**Figure S9**).

To further demonstrate that the composite fibers could be knitted into a readily wearable textile device, we used four-ply yarn and knitted them into an elbow sleeve (**Figure 7a**). The elbow sleeve was designed such that the MXene/PU fiber was knitted into a patch (~35 mm × ~8 mm) over the elbow to enable the textile sensor to stretch during bending of the wearer's arm and to relax upon straightening. The outer portion of the band was knitted with nylon, spandex, and polyester fibers to provide comfort and flexibility. This elbow sleeve was worn on the elbow of a volunteer to demonstrate its use for body movement monitoring (**Figure 7b**). By connecting the knitted fabric sensor to a commercial wireless transmitter (Shimmer[TM]), we were able to monitor the sensing response (voltage) of the elbow sleeve on a personal computer through a wireless Bluetooth® connection (**Figure S10**). Bending the elbow to 90° stretched the fabric sensor by ~50 % and consequently the sensing response decreased (**Figure 7c-d**). Straightening the elbow resulted in the sensing response to increase and return to its original value. We observed that the elbow sleeve could monitor diverse movements of elbow including sudden and relatively fast movements (frequency of ~0.7 Hz). The ability of the textile sensor

to respond to fast movements is essential for practical applications such as sports coaching or injury prevention.
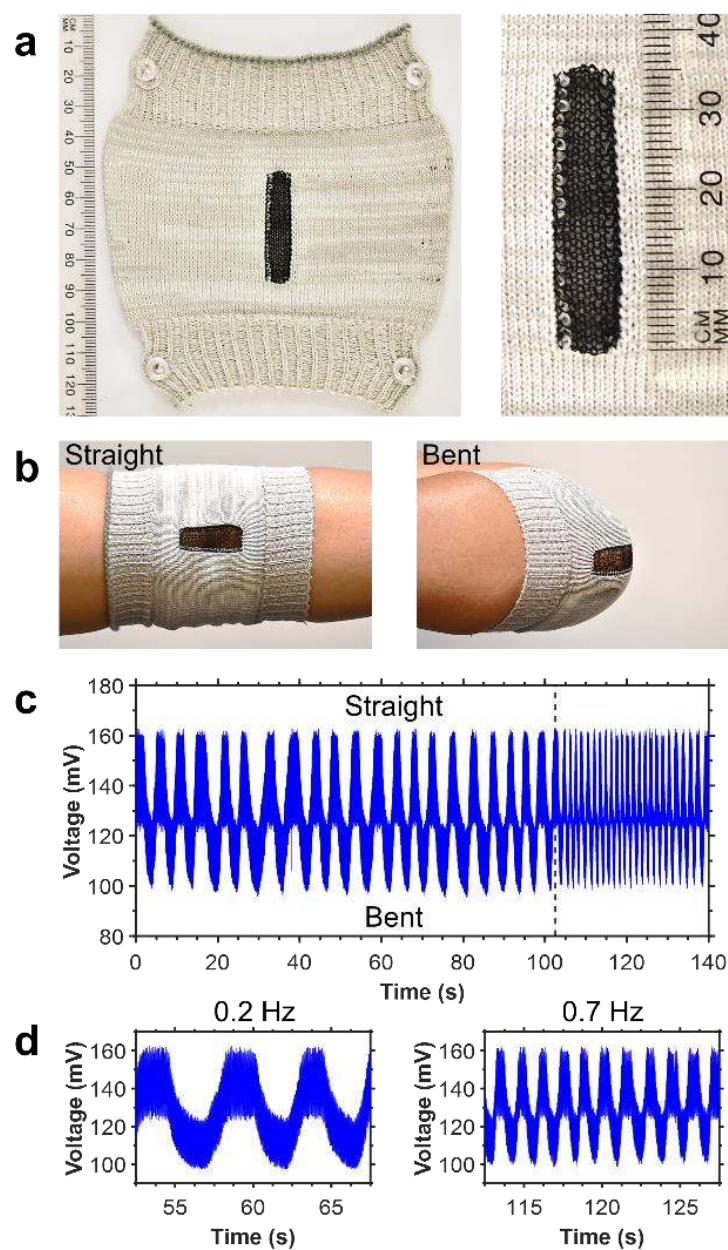

Figure 7. Elbow sleeve knitted by using four-ply yarn of MXene/PU composite fiber a) as-knitted and b) on an elbow at straight and bent conditions. c-d) Strain sensing response of the elbow sleeve recorded while repeatedly bending and straightening the elbow at two different frequencies through a wireless Bluetooth® connection.

22

3. Conclusions

We demonstrated continuous production of MXene/PU composite and coaxial fibers with high conductivity and stretchability that could be knitted into textiles using a commercial-scale knitting machine. Our MXene/PU composite fibers displayed the lowest percolation threshold (~1 wt.%) among other MXene-based composites and the highest rate of reinforcement (~20.3 GPa) among other PU-based composite fibers. We showed that MXene/PU composite fibers could sense strains as high as ~152 % with a very high gauge factor of ~12900. We produced fibers with MXene/PU sheath and PU core by coaxial wet-spinning, which showed an enhanced stability in the cyclic stretching-releasing deformations at various applied strains compared to the non-coaxial composite fiber. We further demonstrated that the MXene/PU fibers had sufficient mechanical properties for machine knitting into textiles with defined loop patterns. The single jersey knit of MXene/PU four-ply yarn could sense strains up to 200 % with excellent stability over 1000 stretching-releasing deformations. Using the MXene/PU fibers, we also knitted an elbow sleeve which could be worn on a user's elbow to track its various movements by sending the signal wirelessly to a personal computer. This work provides detailed insights into the behavior of MXene in elastomeric composites which can be used in other composite systems to achieve electrical and mechanical properties as required for practical applications. The MXene-based strain sensing fibers and textiles developed in this work offer a practical platform for a range of wearable applications requiring body movement monitoring, such as sports coaching, rehabilitation, and injury prevention, remote health monitoring of patients, soft robotics, virtual reality, and entertainment.

4. Experimental

4.1. Synthesis of $Ti_3C_2T_x$ MXene

$Ti_3C_2T_x$ MXene was synthesized using the minimally intensive layer delamination (MILD) method.[13] LiF (4.8 g) was dissolved in HCl (9 M, 60 mL) in a polytetrafluoroethylene bottle. Ti_3AlC_2 MAX phase powder (Carbon-Ukraine, <38 μm particle size, 3 g) was then slowly added to the solution. The mixture was kept stirring at room temperature for 24 h and then washed several times using centrifugation (Thermo Scientific Sorvall ST40) at 3500 rpm for 5 minutes until self-delamination occurred (pH of the supernatant ~6). The sediment was collected in the next step and re-dispersed in water. The mixture was centrifuged at 3500 rpm for 15 min and the supernatant that consisted of highly delaminated $Ti_3C_2T_x$ MXene dispersion was collected.

The aqueous MXene dispersion was transferred into dimethyl sulfoxide (DMSO) or dimethylformamide (DMF) via a solvent exchange method[33] using repeated centrifugation (Thermo Scientific Sorvall ST40) of the parent MXene dispersion at 9000 rpm for one hour. After each centrifugation step, the supernatant was removed and replaced with DMSO or DMF, and the sediment was redispersed using a vortex mixer and manual shaking. This process was repeated three times to maximize water removal.

4.2. Wet-spinning of MXene/PU composite fibers

The MXene/polyurethane (PU) spinning formulations were prepared by dissolving PU (AdvanSource Biomaterials Chronoflex® C 80A) granules in MXene dispersions in DMSO using stirring. Various MXene concentrations are used to achieve MXene loadings of 0 – 100 wt.% (**Table S1**). A custom-built wet-spinning line[16–21] was used to produce MXene/PU fibers. The spinning formulation was injected into a coagulation bath of isopropanol (IPA) or acetic acid (AcOH) through a blunt-tip needle with 23 gauge for IPA or 25 gauge for AcOH as

spinneret. A syringe pump was used to control the flow rate (1-3 mL min^{-1}). After coagulation, the fibers were continuously collected onto a spool and dried in air.

4.3.   Wet-spinning of MXene/PU coaxial fibers

MXene/PU coaxial fibers were produced by using a custom-designed spinneret made by carefully placing a fine needle (25 gauge) inside a larger needle (18 gauge). Coaxial fibers made of MXene sheath and PU core were obtained by injecting the pure PU solution through the inner needle and the MXene/PU formulation through the outer needle of the spinneret. Here, AcOH was used as the coagulation bath and the flow rates of the formulation in the inner and outer needles were controlled (1-2 mL min^{-1}) by using a syringe pump.

4.4.   Knitting MXene/PU fibers into textiles and fabrics

MXene/PU fibers were knitted on a flat-bed knitting machine (Shima Seiki 15 gauge SWG-041N). Textile patches and devices were programed and simulated using Shima Seiki's SDS-ONE APEX3 design system. The sensing elbow sleeve was knitted in one piece, where the sensing component consisted of MXene/PU four-ply yarn and the surrounding fabric consisted of nylon/spandex fibers (NILIT) and polyester yarn (REPREVE).

4.5.   Characterizations

The flake size distributions of the MXene dispersions were measured using dynamic light scattering (DLS) in a Zetasizer (Malvern Instruments, Nano ZS). The viscosity of spinning formulations was measured by a rheometer (TA Instruments Discovery HR-3) at 20 ℃ in parallel plate configuration using a Peltier plate with a diameter of 20 mm. The cross-section morphology of the MXene/PU fibers was observed by a scanning electron microscope (SEM Zeiss Supra 50 VP) after sputter coating with platinum/palladium for 30 s (Cressington Scientific, 108 Auto). Cross-section surfaces were prepared by immersing the fiber in liquid nitrogen for 30 s and breaking the frozen fiber. The diameter of the fiber samples for electrical

and mechanical properties testing was measured using an optical microscope (Olympus BX51) across the whole length of the fiber. The electrical conductivity of the MXene/PU fibers was measured using an in-house four-point probe cell (probe spacing ~230 μm) under laboratory humidity and temperature conditions. A source meter unit (Keithley 2400) was used to apply different currents (I) between two outer probes and the resulting voltages (V) were measured between the two inner probes. Resistance values were then calculated from the I-V curves and used to estimate the electrical conductivity.

The mechanical properties of the MXene/PU fibers were measured using a tensile testing instrument (Instron 3365) equipped with a 5 N (fibers) or a 100 N (textiles) load cell. Fiber samples were prepared by fixing the fiber onto laser-cut paper frames (10 mm aperture). The tensile tests were carried out at strain rates ranging from 1-200 % min^{-1} such that the failure occurred within 1-2 min. A custom-coded program in MATLAB® was used to calculate Young's modulus, tensile strength, and strain at break values from the tensile test data.

The electromechanical properties of the MXene/PU fibers and knitted textiles were measured by real-time monitoring of the resistance using a digital multimeter (Keysight 34461A) during tensile or cyclic extension-relaxation mechanical tests. Samples were prepared by placing a copper tape at each end of the fiber or textile prior to mounting onto the grips. Electromechanical tensile tests were used to calculate sensing range and gauge factor (GF) values (equation 1) from resistance (R) at each applied strain (ε, expressed as percentage) and the initial resistance (R_0, resistance at unstretched state). Two types of cyclic extension-relaxation tests were carried out to measure sensors' sensitivity at various strains and stability. For the sensitivity test, the sample was cyclically stretched (loading) to different applied strain magnitudes (up to 200 %) in 10 % incremental steps and then allowed to relax to zero strain (unloading). The test was repeated at each strain magnitude for 20 cycles. The stability test was

carried out by cyclically stretching the sample to 50 % strain and then allowing it to relax to zero strain for 1000 cycles. The cyclic extension-relaxation tests were carried out at the strain rate of 100 % min^{-1} and a 30 s relaxation time was introduced after each loading and unloading step to allow the resistance of the sample to stabilize. The electromechanical results were analyzed by using custom-coded programs in MATLAB®, which measured R_0, loading resistance (R_L) and unloading resistance (R_U) at each cycle.

$$GF = \frac{R - R_0}{\varepsilon R_0} \times 100 \qquad (1)$$

Wireless body movement monitoring experiments were performed on the knitted elbow sleeve worn on an elbow of a volunteer. The knitted fabric sensor was connected to a commercial wireless transmitter (Shimmer^{TM} 3) via a voltage divider circuit (using 1 MΩ and 1 kΩ resistors) and the voltage signal was transmitted to a personal computer using Bluetooth® connection. The test was carried out by cyclically bending and straightening the elbow of the wearer and the sensing data was recorded real-time.

Supporting Information

Supporting Information is available from the Wiley Online Library or from the authors.

Received: ((will be filled in by the editorial staff))

Revised: ((will be filled in by the editorial staff))

Published online: ((will be filled in by the editorial staff))

References

[1]   B. Anasori, Y. Gogotsi, *2D Metal Carbides and Nitrides (MXenes)*; Springer International Publishing: Cham, 2019.

[2]   M. Naguib, V. N. Mochalin, M. W. Barsoum, Y. Gogotsi, *Adv. Mater.* **2014**, *26*, 992.

[3]   Z. Ling, C. E. Ren, M. Zhao, J. Yang, J. M. Giammarco, J. Qiu, *Proc. Natl. Acad. Sci. U. S. A.* **2014**, *111*, 16676.

[4]   B. Anasori, M. R. Lukatskaya, Y. Gogotsi, *Nat. Rev. Mater.* **2017**, *2*, 16098.

[5]   J. Pang, R. G. Mendes, A. Bachmatiuk, L. Zhao, H. Q. Ta, T. Gemming, H. Liu, Z. Liu, M. H. Rummeli, *Chem. Soc. Rev.* **2019**, *48*, 72.

[6]   C. J. Zhang, B. Anasori, A. Seral-Ascaso, S.-H. Park, N. McEvoy, A. Shmeliov, G. S. Duesberg, J. N. Coleman, Y. Gogotsi, V. Nicolosi, *Adv. Mater.* **2017**, *29*, 1702678.

[7]   A. Lipatov, H. Lu, M. Alhabeb, B. Anasori, A. Gruverman, Y. Gogotsi, A. Sinitskii, *Sci.*

Adv. **2018**, *4*, eaat0491.

[8]   M. R. Lukatskaya, S. Kota, Z. Lin, M. Zhao, N. Shpigel, M. D. Levi, J. Halim, P. Taberna, M. W. Barsoum, P. Simon, Y. Gogotsi, *Nat. Energy* **2017**, *17105*, 1.

[9]   Z. Li, Y. Cui, Z. Wu, C. Milligan, L. Zhou, G. Mitchell, B. Xu, E. Shi, J. T. Miller, F. H. Ribeiro, Y. Wu, *Nat. Catal.* **2018**, *1*, 349.

[10]   S. J. Kim, H.-J. Koh, C. E. Ren, O. Kwon, K. Maleski, S.-Y. Cho, B. Anasori, C.-K. Kim, Y.-K. Choi, J. Kim, Y. Gogotsi, H.-T. Jung, *ACS Nano* **2018**, *12*, 986.

[11]   A. Sarycheva, A. Polemi, Y. Liu, K. Dandekar, B. Anasori, Y. Gogotsi, *Sci. Adv.* **2018**, *4*, eaau0920.

[12]   N. Driscoll, A. G. Richardson, K. Maleski, B. Anasori, O. Adewole, P. Lelyukh, L. Escobedo, D. K. Cullen, T. H. Lucas, Y. Gogotsi, F. Vitale, *ACS Nano* **2018**, *12*, 10419.

[13]   M. Alhabeb, K. Maleski, B. Anasori, P. Lelyukh, L. Clark, S. Sin, Y. Gogotsi, *Chem. Mater.* **2017**, *29*, 7633.

[14]   F. Shahzad, M. Alhabeb, C. B. Hatter, B. Anasori, S. Man Hong, C. M. Koo, Y. Gogotsi, *Science* **2016**, *353*, 1137.

[15]   A. J. Granero, P. Wagner, K. Wagner, J. M. Razal, G. G. Wallace, M. in het Panhuis, *Adv. Funct. Mater.* **2011**, *21*, 955.

[16]   M. Z. Seyedin, J. M. Razal, P. C. Innis, G. G. Wallace, *Adv. Funct. Mater.* **2014**, *24*, 2957.

[17]   S. Seyedin, J. M. Razal, P. C. Innis, A. Jeiranikhameneh, S. Beirne, G. G. Wallace, *ACS Appl. Mater. Interfaces* **2015**, *7*, 21150.

[18]   S. Seyedin, S. Moradi, C. Singh, J. M. Razal, *Appl. Mater. Today* **2018**, *11*, 255.

[19]   S. Seyedin, J. M. Razal, P. C. Innis, G. G. Wallace, *Smart Mater. Struct.* **2016**, *25*, 035015.

[20]   M. Z. Seyedin, J. M. Razal, P. C. Innis, R. Jalili, G. G. Wallace, *Adv. Funct. Mater.* **2015**, *25*, 94.

[21]   S. Seyedin, J. M. Razal, P. C. Innis, R. Jalili, G. G. Wallace, *Adv. Mater. Interfaces* **2016**, *3*, 1500672.

[22]   S. Lee, S. Shin, S. Lee, J. Seo, J. Lee, S. Son, H. J. Cho, H. Algadi, S. Al-Sayari, D. E. Kim, T. Lee, *Adv. Funct. Mater.* **2015**, *25*, 3114.

[23]   Y. Lu, J. Jiang, S. Yoon, K.-S. Kim, J.-H. Kim, S. Park, S.-H. Kim, L. Piao, *ACS Appl. Mater. Interfaces* **2018**, *10*, 2093.

[24]   S. Seyedin, P. Zhang, M. Naebe, S. Qin, J. Chen, X. Wang, J. M. Razal, *Mater. Horizons* **2019**, *6*, 219.

[25]   S. Seyedin, E. R. S. Yanza, J. M. Razal, *J. Mater. Chem. A* **2017**, *5*, 24076.

[26]   J. Zhang, S. Seyedin, Z. Gu, W. Yang, X. Wang, J. M. Razal, *Nanoscale* **2017**, *9*, 18604.

[27]   Z. Wang, S. Qin, S. Seyedin, J. Zhang, J. Wang, A. Levitt, N. Li, C. Haines, R. Ovalle-Robles, W. Lei, Y. Gogotsi, R. H. Baughman, J. M. Razal, *Small* **2018**, *14*, 1802225.

[28]   J. Zhang, S. Seyedin, S. Qin, Z. Wang, S. Moradi, F. Yang, P. A. Lynch, W. Yang, J. Liu, X. Wang, J. M. Razal, *Small* **2019**, *15*, 1804732.

[29]   A. S. Levitt, M. Alhabeb, C. B. Hatter, A. Sarycheva, G. Dion, Y. Gogotsi, *J. Mater. Chem. A* **2019**, *7*, 269.

[30] W. T. Cao, F. F. Chen, Y. J. Zhu, Y. G. Zhang, Y. Y. Jiang, M. G. Ma, F. Chen, *ACS Nano* **2018**, *12*, 4583.

[31] M. Naguib, T. Saito, S. Lai, M. S. Rager, T. Aytug, M. Parans Paranthaman, M.-Q. Zhao, Y. Gogotsi, *RSC Adv.* **2016**, *6*, 72069.

[32] W. Zhi, S. Xiang, R. Bian, R. Lin, K. Wu, T. Wang, D. Cai, *Compos. Sci. Technol.* **2018**, *168*, 404.

[33] S. Seyedin, J. Zhang, K. A. S. Usman, S. Qin, A. M. Glushenkov, E. R. S. Yanza, R. T. Jones, J. M. Razal, *Glob. Challenges* **2019**, *3*, 1900037.

[34] O. Mashtalir, M. Naguib, V. N. Mochalin, Y. Dall'Agnese, M. Heon, M. W. Barsoum, Y. Gogotsi, *Nat. Commun.* **2013**, *4*, 1716.

[35] A. Ziabicki, *Fundamentals of Fibre Formation: The Science of Fibre Spinning and Drawing*; Wiley: London, 1976.

[36] K. Maleski, V. N. Mochalin, Y. Gogotsi, *Chem. Mater.* **2017**, *29*, 1632.

[37] Z. S. Petrović, J. Ferguson, *Prog. Polym. Sci.* **1991**, *16*, 695.

[38] F. Yeh, B. S. Hsiao, B. B. Sauer, S. Michel, H. W. Siesler, *Macromolecules* **2003**, *36*, 1940.

[39] E. M. Christenson, J. M. Anderson, A. Hiltner, E. Baer, *Polymer* **2005**, *46*, 11744.

[40] H. J. Qi, M. C. Boyce, *Mech. Mater.* **2005**, *37*, 817.

[41] M. Szycher, *Szycher's Handbook of Polyurethanes*; Second Edi.; CRC Press: Boca Raton, 2013.

[42]   H. Koerner, W. Liu, M. Alexander, P. Mirau, H. Dowty, R. A. Vaia, *Polymer* **2005**, *46*, 4405.

[43]   A. Voet, *J. Polym. Sci. Macromol. Rev.* **1980**, *15*, 327.

[44]   G. Huber, *Macromolecules* **2002**, *35*, 9204.

[45]   L. Bokobza, *Macromol. Mater. Eng.* **2004**, *289*, 607.

[46]   J. N. Coleman, U. Khan, W. Blau, Y. Gunko, *Carbon* **2006**, *44*, 1624.

[47]   J. J. Park, W. J. Hyun, S. C. Mun, Y. T. Park, O. O. Park, *ACS Appl. Mater. Interfaces* **2015**, *7*, 6317.

[48]   T. Yamada, Y. Hayamizu, Y. Yamamoto, Y. Yomogida, A. Izadi-Najafabadi, D. N. Futaba, K. Hata, *Nat. Nanotechnol.* **2011**, *6*, 296.

[49]   O. Atalay, W. Kennon, *Sensors* **2014**, *14*, 4712.

[50]   J. Foroughi, G. M. Spinks, S. Aziz, A. Mirabedini, A. Jeiranikhameneh, G. G. Wallace, M. E. Kozlov, R. H. Baughman, *ACS Nano* **2016**, *10*, 9129.

WILEY-VCH

Conductive elastomeric composite and coaxial fibers are fabricated using $Ti_3C_2T_x$ MXene, which show strain sensing properties by changing electrical resistance when stretched. Using industrial-scale knitting machine, the composite fibers are knitted into strain sensing textiles that can be worn directly and monitor the user's diverse body movements. MXene-based fibers and textiles can cater for wearable applications such as off-site health monitoring of patients.

Keyword: MXene fiber strain sensor

MXene Composite and Coaxial Fibers with High Stretchability and Conductivity for Wearable Strain Sensing Textiles

Shayan Seyedin,* Simge Uzun, Ariana Levitt, Babak Anasori, Genevieve Dion, Yury Gogotsi,* and Joselito M. Razal*